Entanglement Constraints in Polymer Melts. A Neutron Spin Echo Study

D. Richter*

Institut für Festkörperforschung, Forschungszentrum Jülich, 5170 Jülich, Germany

R. Butera,† L. J. Fetters, and J. S. Huang

Exxon Research and Engineering Company, Corporate Research Laboratories, Annandale, New Jersey 08801

B. Farago

Institut Laue-Langevin, 38042 Grenoble, France

B. Ewen

Max-Planck-Institut für Polymerforschung, 6500 Mainz, Germany

Received December 24, 1991; Revised Manuscript Received July 22, 1992

ABSTRACT: Using neutron spin echo spectroscopy, we have studied the melt dynamics of polyisoprene (PI), saturated polybutadiene (PEB-2), and poly(ethylene–propylene) alternating copolymer (PEP). The experiments on all three polymers show that beyond a characteristic length d and after a crossover time τ_e the relaxational density fluctuations within a given chain are strongly impeded. The presence of an intermediate dynamic length scale in the chain dynamics establishes the microscopic existence of a well-defined entanglement distance confirming thereby one of the essential assumptions of the reptation concept. The microscopically determined lengths agree well with those obtained from the plateau moduli if interpreted in terms of the reptation theory. The detailed line shape of the dynamic structure factor supports the concept of local reptation.

1. Introduction

The viscoelasticity of long-chain polymer melts displays a series of unusual properties, the most spectacular of which is the presence of a broad plateau regime in the dynamic modulus $G'(\omega)$.[1-3] In this time or frequency regime $G'(\omega)$ is constant and consequently the polymer melt exhibits elastic behavior similar to a rubber, where elasticity arises from the conformational entropy of chains between the permanent cross-links. Therefore, it was assumed that in dense polymer systems the interpenetrating chains mutually impose long-lived topological constraints acting like temporary cross-links. Then in analogy to elastomers, the plateau in the dynamic modulus results from the entropy elasticity of the chains between these entanglements.

Among the theoretical approaches[4-12] addressing the viscoelastic properties of dense polymer systems the reptation model stands out as being to date the most complete and most successful theory.[4,5] It assumes that large scale transverse motions with respect to the course grained chain contour are supressed by the presence of the entanglements. The geometrical constraints are then modeled by a tube confinement surrounding a given chain mandating snakelike motion along the chain profile. With the tube diameter d, which may be identified with the distance between entanglements, the reptation model introduces a new intermediate dynamic length scale, larger than the segment length but for long chains much smaller than the chain dimension. Being a truly dynamic length, d cannot be observed by static experiments. Therefore, in spite of its fundamental importance for a molecular understanding of viscoelasticity, its direct microscopic observation, though attempted,[13-15] remained elusive until very recently.[16,17]

† Present address: du Pont Marshall Laboratory, 3500 Grays Ferry Ave., Philadelphia, PA 19146.

In order to observe the spatially constrained motion of chain segments in dense environments, quasielastic neutron scattering (QNS) is a unique probe. This is partly due to the fact that by hydrogen–deuterium exchange the scattering contrast of polymers can be changed thus allowing the observation of a single chain among others. Second, since with cold neutrons the obtainable momentum and energy transfers correspond to intramolecular distances *and* relaxation times, QNS accesses simultaneously the space *and* time evolution of the intramolecular motion.[18] In particular neutron spin echo (NSE) spectroscopy is well suited for the observation of slow large-scale motion since it provides high-energy resolution in the small-angle scattering regime. Furthermore it accesses the intermediate dynamic structure factor which directly describes the time-dependent relaxation behavior we are interested in.

Here we give an account of our NSE studies of the dynamic structure factors of three different polymers: poly(ethylene–propylene) alternating copolymer (PEP), saturated polybutadiene (PEB-2), and polyisoprene (PI). The objective of these experiments was to establish the microscopic existence of the entanglement distance and to relate it to the rheological results.

2. Dynamic Structure Factors

In this section we outline theoretical models for chain motion in dense environments. We give a short account of the Rouse model[19] treating the effect of entropic forces on the chain motion. We consider the consequences of the tube confinement on the segmental dynamics and display the basic features of the reptation model.[4,5] An experimental test of these models by QNS needs the calculation of the corresponding dynamic structure factors $S(Q,t)$, where Q is the momentum transfer during scattering ($Q = (4\pi/\lambda)\sin\theta$, where λ is the neutron wavelength

0024-9297/92/2225-6156$03.00/0 © 1992 American Chemical Society

and 2θ is the scattering angle) and t is the time, containing the desired space time information. We present $S(Q,t)$ for Rouse motion[20] and discuss approaches to calculate $S(Q,t)$ for reptation in the so-called local reptation model[21] and a heuristic effective medium model.[7]

If chains could intersect freely, the chain dynamics would be described as thermal motion damped via a friction coefficient ζ. This so-called Rouse model[19] considers a Gaussian chain of N segments with a length l in a heat bath and explores the effect of entropic forces on the chain motion. For times much shorter than the longest relaxation time, the Rouse time $\tau_R = \zeta N^2 l^2/3\pi^2 k_B T$ (k_B is the Boltzmann factor; T is temperature), the mean square segment displacement Δr_{nn}^2 follows[20] a fractal time dependence

$$\Delta r_{nn}^2 = 2l^2(3k_BTt/\pi\zeta l^2)^{1/2} \tag{1}$$

In the Gaussian approximation the segment self-correlation function relates directly to the mean square segment displacement. In the neutron spin echo experiments we investigated the spatial Fourier transform of the pair correlation function

$$S(Q,t) = \frac{1}{N}\sum_{i,j} \exp\left[-\frac{Q^2}{6}\langle(\mathbf{r}_j(t) - \mathbf{r}_i(0))^2\rangle\right] \tag{2}$$

where $\mathbf{r}_i$ and $\mathbf{r}_j$ are the position vectors of the segments "i" and "j". The parantheses represent the thermal mean. The pair correlation function correlates the position of segment i at a time t with that of a segment j of the same chain at $t = 0$ and is more complicated than the self-correlation function.[20] We note, however, that as the self-correlation function for $t < \tau_R$, it scales with one scaling variable $u = Q^2 l^2 \sqrt{3k_BT/l^2\zeta t} = Ql^2\sqrt{Wt}$ (W is the Rouse rate) which we call the Rouse variable. The $Q - t$ scaling results from the fact that besides the cutoff length scales R_g (size of the chain) and l, the model does not contain any length scale. The characteristic decay rate of $S(Q,t)/S(Q,0)$ is given by

$$\Omega_R = \frac{1}{12}\frac{k_BT}{\zeta} l^2 Q^4 \tag{3}$$

In the *reptation model* the tube confinement expressed by the tube diameter d leads to strong alterations of the mean square segment displacements as compared to the Rouse model. (i) For short times during which a chain segment does not notice any of the topological restrictions of the movement ($r < d$), we expect unrestricted Rouse behavior $\Delta r_{nn}^2(t) \sim t^{1/2}$. This motional behavior reaches its limits of Δr_{nn}^2 becomes comparable with the tube diameter d^2. With the aid of (1) and the condition $\Delta r_{nn}^2 = d^2$ it follows for the crossover time

$$\tau_e = \frac{\pi}{12}\frac{d^4\zeta}{k_BTl^2} \tag{4a}$$

A different estimate which identifies τ_e with the slowest Rouse mode of a chain with the end-to-end distance $R_e^2 = d^2$ leads to the same result

$$\tau_e = \frac{1}{3\pi^2}\frac{d^4\zeta}{k_BTl^2} \tag{4b}$$

except for factors. (ii) For times $t > \tau_e$ was have to consider curve–linear Rouse motion along the spatially fixed tube. Two different time regimes have to be distinguished. For ($t < \tau_R$) the Rouse modes equilibrate along the tube and we retain the familiar $t^{1/2}$ law, while for $t > \tau_R$ the chain diffuses along the tube. If a segment performs a mean square displacement along the tube, its mean square displacement in 3-D space is given by the square root of its value along the tube—after all the tube itself constitutes a Gaussian random-walk. For the two regimes we thus obtain

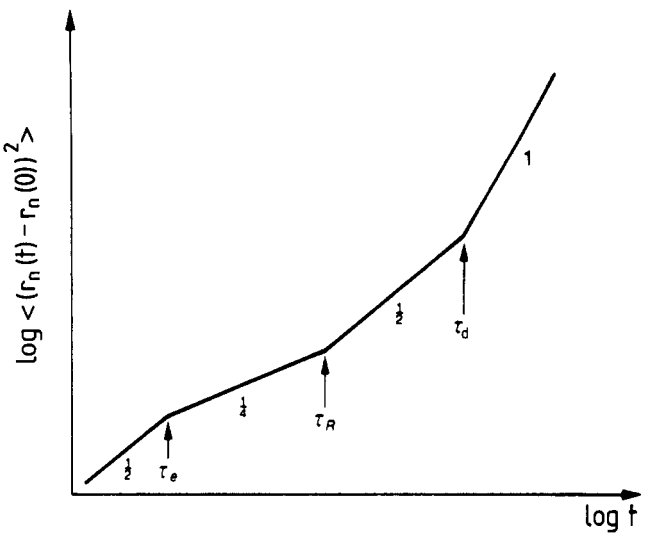

Figure 1. Mean square displacement of a chain segment undergoing reptational motion as a function of time.

$$\Delta r_{nn}^2(t) = d\left(\frac{k_BTl^2}{\zeta}t\right)^{1/4} \qquad t < \tau_R$$

$$\Delta r_{nn}^2(t) = d\left(\frac{k_BTt}{N\zeta}\right)^{1/2} \qquad \tau_d > t > \tau_R \tag{5}$$

where τ_d is the terminal time at which the chain has left its original tube. (iii) For times $t > \tau_d \simeq N^3\zeta l^4/k_BTd^2$ the dynamics are determined by reptation diffusion. We expect normal diffusive behavior $\Delta r_{nn}^2(t) \simeq (k_BTd^2/N^2l^2\zeta)t$. The reptation model thus predicts four dynamical regimes for segment diffusion. They are summarized in Figure 1.

In the case of the reptational motion the calculation of the pair correlation function is rather problematic. We shall remind ourselves of the problem on the basis of Figure 2. The figure gives a diagrammatic representation of the reptation process during various characteristic time intervals: (i) For $t < \tau_e$ we are dealing with unrestricted Rouse movements. Here the dynamic structure factor of the Rouse model should be valid. For $t = \tau_e$ density fluctuations are equilibrated within a chain over the linear scale of the tube diameter. (ii) For $t > \tau_e$ we are, according to De Gennes, in the regime of local reptation.[21] Density fluctuations are equilibrated within the chain along the solid tube. Here, the $t^{1/4}$ law is valid for the self-correlation function. The pair correlation function is sensitive to changes of the relative position of different segments. During Rouse relaxation in the solid tube the relative arrangements of segments change only marginally—to a large extent they slip collectively up and down the tube. For the dynamic structure factor this means that $S(Q,t)$ tends to approach a constant plateau value. (iii) For $\tau_R < t < \tau_d$ the chain creeps out of its tube. Here τ_d is the time after which the chain has left its original tube. Correlations between the various chain segments are gradually lost. We here expect a further decrease of $S(Q,t)$. (vi) For $t > \tau_d$, the segment diffusion process is converted into reptation diffusion. Normal diffusive behavior, determined by the reptation diffusion constant, can be expected here.

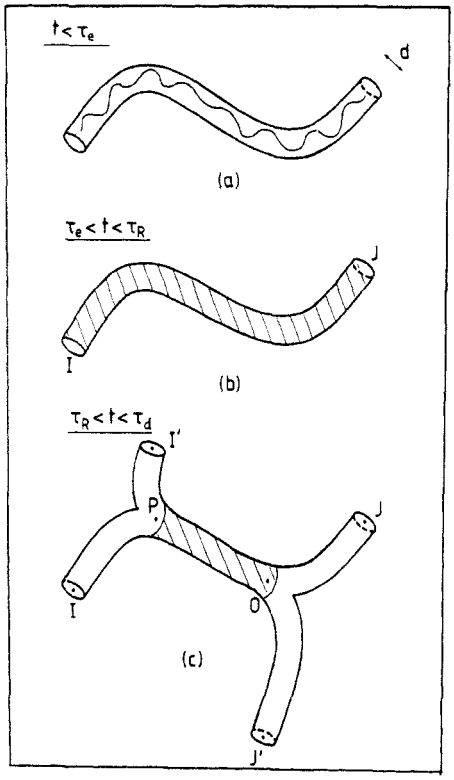

Figure 2. *Schematic representation of a reptating chain in different time regimes: (a) short-time unrestricted Rouse motion; (b) equilibrium of density fluctuations along the chain; (c) creep motion of chain out of tube.*

We have already dealt with domain i. For the regime of local reptation ($t > \tau_e$) a calculation by De Gennes gives $S(Q,t)$ to first order of $(Qd)^2$ [21]

$$S(Q,t) = 1 - \frac{Q^2d^2}{36} + \frac{Q^2d^2}{36}\exp\left(\frac{u^2}{36}\right)\mathrm{erfc}\left(\frac{u}{6}\right) \qquad (6)$$

where u is the "Rouse variable". $S(Q,t)$ describes the equilibration of density fluctuations along the tube (local reptation). The important feature of eq 6 is the factor Qd which introduces the new length scale. Due to the tube constraints, $S(Q,t)$ only partially decays to a certain Q-dependent fraction. The remaining "elastic" part is a consequence of long-lived segment–segment correlation due to the tube confinement. The elastic part actually decays only for times in the order of the terminal time τ_d. The existence of the tube diameter as a dynamic characteristic length breaks up the scaling property of the Rouse model, $S(Q,t) = S(Q^2t^{1/2})$, and leads to characteristic deviations. (Apart from the dependence on $Q^2t^{1/2}$, $S(Q,t)$ depends explicitly on Qd.) This result is of a general nature and does not depend on the special De Gennes model. Finally eq 6 does not consider correctly the initial Rouse relaxation which should prevail as long as the segment displacements are smaller than the tube diameter.

A quantitative analysis of scattering data originating from the crossover regime between short-time Rouse and entanglement-controlled motion needs an explicit consideration of the initial Rouse relaxation neglected by De Gennes. The only model in the literature providing an analytic expression for $S(Q,t)$ in this regime is Ronca's effective medium approach.[7] In the framework of the self-consistent approach of Hess[9] and the reptation model, Ronca's model is a simplification using an ad hoc approach for the time-dependent friction. For the transition region to entanglement-controlled behavior, Ronca's approach leads to an explicit analytic form for $S(Q,t)$. Clear deviations from the dynamic structure factor of the Rouse model can be seen even for $Qd = 7$. This aspect agrees well with computer simulations by Kremer et al.[22,23] who found such deviations in the Q regime $2.9 \leq Qd \leq 6.7$.

Table I
Polymer Molecular Characteristics

sample	$10^{-4}M_w$[a]	M_z/M_w[b]	M_w/M_n[b]
PI-h_8 sample 1	5.7	1.02	1.03
PI-d_8 sample 1	5.2	1.02	1.03
PI-h_8 sample 2	7.40	1.02	1.04
PI-d_8 sample 2	7.91	1.03	1.05
PEP-d_{10}	8.38	1.03	1.05
PEP-h_{10}	8.22	1.02	1.05
PEP triblock	8.78	1.03	1.06
PEB-2-h_8	7.05	1.04	1.04
PEB-2-d_8	7.32	1.02	1.04

[a] Light scattering. [b] Size exclusion chromatography.

Finally the Doi–Edwards theory of viscoelasticity[5] relates the plateau modulus, a property accessible to rheological measurements, to the microscopic tube diameter of the reptation model.[24]

$$G_N^0 = \frac{4}{5}\frac{\langle R_e^2\rangle}{M}\frac{\rho RT}{d^2} \qquad (7)$$

where $\langle R_e^2\rangle = nNC_\infty l_0^2$ is the mean square end-to-end distance, C_∞ is the characteristic ratio, l_0 is the average main-chain bond length, n is the average bond number/monomer, M is the molecular weight, ρ is the polymer density, and R is the gas constant. Equation 7 is one of the fundamental relationships of the Doi–Edwards theory relating macroscopic viscoelastic properties to the microscopic chain confinement.

3. Experimental Section

3.1. Sample Preparation and Characterization. Given the still limited temporal resolution of neutron spin echo ($t < 40$ ns) it was essential to select thermally stable linear polymers combining high flexibility, a large plateau modulus, indicating strong topological constraints, and a low monomeric friction coefficient yielding high segmental mobility. For our experiments we chose 1,4-polyisoprene (PI), the alternating copolymer of poly(ethylene–propylene) (PEP) which was obtained from hydrogenation of 1,4-polyisoprene, and hydrogenated 1,4-polybutadiene (PEB-2) which essentially resembles polyethylene (PE). The different polymer samples including their characteristics are listed in Table I. The plateau modulus of PI of $G_N^0(\mathrm{PI}) = 0.44 \times 10^7$ dynes/cm^2 at room temperature increases by nearly a factor of 3 upon hydrogenation to $G_N^0(\mathrm{PEP}) = 1.22 \times 10^7$ dynes/cm^2. The largest plateau modulus is exhibited by PE amounting to $G_N^0(\mathrm{PE}) = 2.2 \times 10^7$ dynes/cm^2 at 100 °C. Using eq 7 in the framework of the Doi–Edwards theory, the plateau moduli convert to the following entanglement distances $d(\mathrm{PI}) = 51$ Å, $d(\mathrm{PEP}) = 36$ Å, and $d(\mathrm{PE}) = 35$ Å (373 K). The Kuhn lengths of PI at 300 K, PEP at 492 K, and PEB-2 at 509 K are 7.7, 9.2, and 8.6 Å, respectively, indicating high flexibility.[25] Finally, using the Vogel–Fulcher viscosity parameters, we estimate monomeric friction coefficients of $\zeta(\mathrm{PI}) \simeq 1.2 \times 10^{-9}$ (dynes s)/cm at 473 K[26] and $\zeta(\mathrm{PEP}) = 1.9 \times 10^{-9}$ (dynes s)/cm at 500 K.[17] Thereby for the monomer length we used $l^2 = l_0^2nC_\infty$ where $n = 3.86$ is the effective bond number/monomer in PI and PEP. Diffusion experiments on PE gave $\zeta(\mathrm{PE}) \simeq 3 \times 10^{-10}$ (dynes s)/cm at 448 K.[27] The corresponding Rouse rates $W = 3kT/l^2\zeta$ are $W(\mathrm{PI}) = 4.3 \times 10^{10}$ s^{-1} (473 K), $W(\mathrm{PEP}) = 2.2 \times 10^{10}$ s^{-1} (500 K), and $W(\mathrm{PE}) = 5.4 \times 10^{10}$ s^{-1} (448 K), respectively, assuring high mobility.

The polyisoprenes and polybutadienes were prepared via standard anionic polymerization techniques: Purified, by sublimation, *tert*-butyllithium was the initiator. The deuterated monomers were obtained from Cambridge Isotopes. The microstructure (H or D NMR) of the polyisoprenes was 75% cis-1,4, ~18% trans-1,4 and ~7% 3,4, while that of the polybuta-

dienes was ~40% cis-1,4, ~53% trans-1,4 and ~7% 1,2. Size exclusion chromatography was used to evaluate the heterogeneity indices.

The saturation by hydrogen or deuterium of the polydienes was done by using palladium on calcium carbonate. The procedure followed that of Rachapudy et al.[28] NMR analysis showed that saturation levels of >99.7% were obtained. The saturation of polyisoprene yielded essentially alternating amorphous poly(ethylene–propylene) (PEP) while polybutadiene yielded the crystalline poly(ethylene–1-butene) copolymer which is designated as PEB-2 (where the integer denotes the approximate number of ethyl branches per 100 backbone carbons). Densities at 23.1 °C for the amorphous polymers were measured in a density gradient column. Weight-average molecular weights were evaluated via a Chromatix KMX-6 low-angle laser photometer. For the case of the PEB-2 materials the molecular weights of the parent polybutadienes were measured and corrected for saturation.

3.2. Quasielastic Neutron Scattering. The quasielastic neutron-scattering experiments were performed using the neutron spin echo (NSE) spectrometer IN11 at the Institute Laue-Langevin (ILL) in Grenoble. NSE measures the neutron velocities of the incoming and outgoing neutrons utilizing the Larmor precessions of the neutron spin in an external guide field. Since the neutron spin acts like the hand of an "internal clock" attached to each neutron storing the result of the velocity measurement on the neutron itself, neutron velocity differences can be measured directly in studying the final polarization of the neutron beam.[16] As eluded to before, such a measurement accesses the intermediate dynamic structure factor $S(Q,t)/S(Q,0)$. Thereby, the time is proportional to the applied guide field and the neutron wavelength λ^3. Given a certain range of applicable magnetic fields, the time range of the instrument can be enlarged by changing the wavelength. In particular, large neutron wavelengths reach to long times. Using wavelengths up to λ = 11.8 Å, we could achieve times up to t_{max} = 46 ns. Under these circumstances the energy resolution corresponds to ~5 neV (1/e decay). The accessible Q range in the small-angle regime amounts to 0.02 Å$^{-1} \leq Q \leq$ 0.15 Å^{-1} with a Q resolution of about 20%.

The sample cells consisted of tight Nb containers with variable thicknesses between 1 and 4 mm. Loading of the samples took place under inert atmosphere in order to displace oxygen which might degrade the polymers at elevated temperatures. The samples were heated in a vacuum furnace up to 509 K with a temperature stability of ΔT = ±1 °C. All samples contained small fractions of protonated polymers in a deuterated matrix. The backgrounds from the matrices—nearly entirely inelastic scattering—and from the container were measured separately and substracted using the proper transmission factors. Resolution corrections were performed using the instrumental resolution function obtained from a glassy PS standard (90% deuterated/10% hydrogenated) at room temperature.

4. Results

NSE experiments were performed on PI, PEP, and PEB-2 which exhibit an increasing plateau modulus and thus increasing topological constraints. We commence with the results on PI, then present the PEP data and finally show the PEB-2 results.

4.1. Polyisoprene Melts. We investigated two different samples. Sample 1 12% protonated molecules, 2-mm cell; sample 2 containing 10% protonated PI, 2-mm cell (for detailed characteristics see Table I). The experiments were carried out at 195 °C (sample 1) and 200 °C (sample 2). Sample 1 was studied at a neutron wavelength of λ = 8.56 Å, while sample 2 was investigated at λ = 8.5 Å and λ = 11.8 Å, respectively; the latter allowed the attainment of maximum time of t = 46 ns.

Figure 3 presents the measured dynamic structure factor from sample 1 for different momentum transfers. The solid lines represent a fit with the dynamic structure factor of the Rouse model where we restricted the time regime of the fit to the initial part. At short times the data are well represented by the solid lines while at longer times deviations toward slower relaxation are obvious. In order to further demonstrate the quality of the Rouse description for the initial decay, Figure 4 presents the Q dependence of the characteristic frequency in a double-logarithmic plot. The solid line displays the $\Omega_R \sim Q^4$ law as given by eq 3. Over the entire Q range within experimental error the data points fall on the line and thus exhibit the predicted Q^4 dependence. A similar result has recently been reported for PDMS,[15] where the geometrical constraints are apparently even less pronounced than for PI. The insert in Figure 4 demonstrates the scaling behavior of the experimental spectra which according to the Rouse model are required to collapse to one master curve if they are plotted in terms of the Rouse variable $u = Q^2l^2\sqrt{Wt}$. The solid line displays the result of a joint fit to the Rouse structure factor with the only fitted parameter being Wl^4. An excellent agreement with the theoretical prediction is observed. The resulting value is Wl^4 = (2.0 ± 0.1) × 10^{13} Å^4 s^{-1}. Similarly, the data obtained from sample 2 were evaluated in the short time range in order

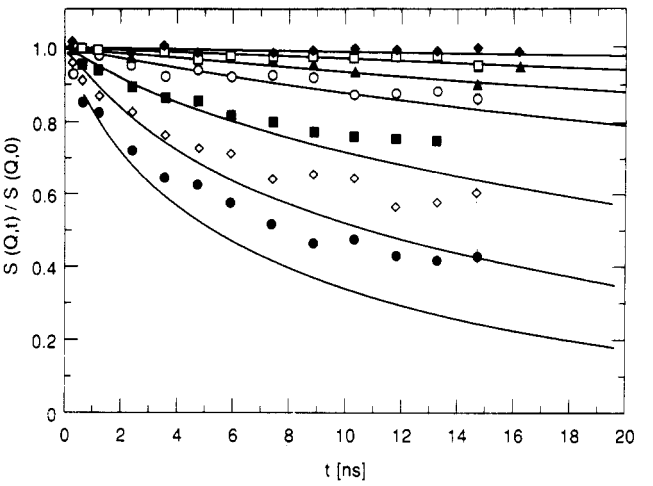

Figure 3. Dynamic structure factor as observed from PI sample 1 for different momentum transfers at 468 K: (◆) Q = 0.038 Å^{-1}; (□) Q = 0.051 Å^{-1}; (▲) Q = 0.064 Å^{-1}; (○) Q = 0.077 Å^{-1}; (■) Q = 0.102 Å^{-1}; (◇) Q = 0.128 Å^{-1}; (●) Q = 0.153 Å^{-1}. The solid lines display fits with the Rouse model to the initial decay.

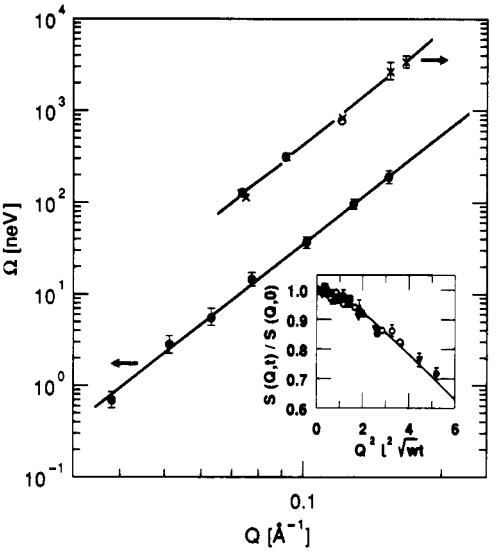

Figure 4. Characteristic frequency for the Rouse decay for the PI samples as function of Q: (●) sample 1; sample 2 (×) λ = 8.5 Å, (○) λ = 11.8 Å. The insert displays the scaling behavior of dynamic structure factor if plotted vs the Rouse scaling variable $Q^2l^2\sqrt{Wt}$. The different symbols corresponds to different Q values.

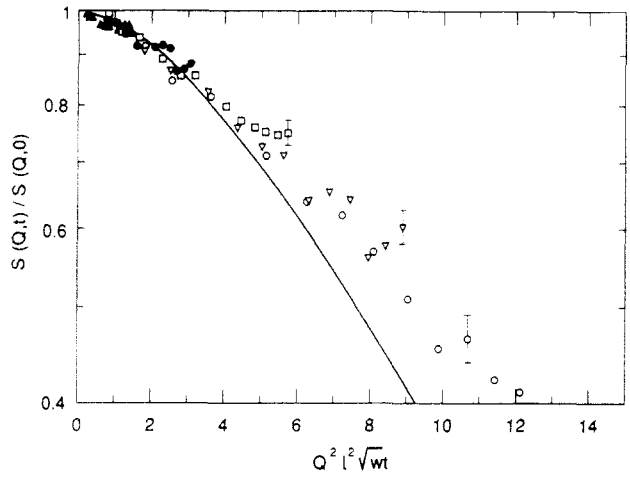

Figure 5. Scaling representation of the spectra obtained from the PI sample 1 in terms of the Rouse variable: (○) Q = 0.153 Å^{-1}; (▽) Q = 0.128 Å^{-1}; (□) Q = 0.102 Å^{-1}; (●) Q = 0.077 Å^{-1}; (▲) Q = 0.064 Å^{-1}. The solid line displays the Rouse structure factor using the Rouse rate determined at short times.

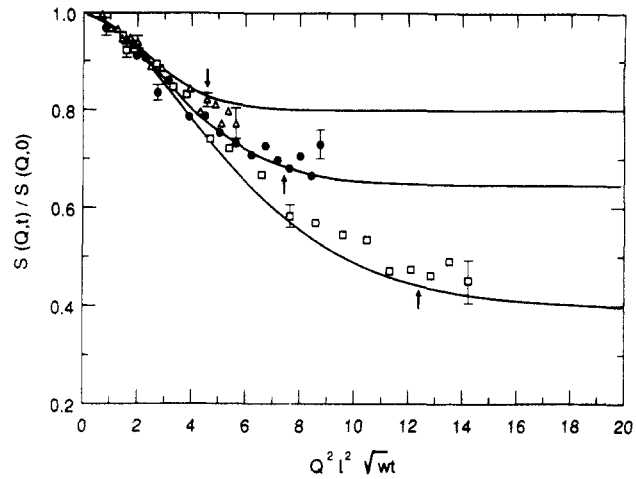

Figure 6. Rouse-scaling representation of the spectra obtained from the PI sample 2 at λ = 11.8 Å and T = 473 K: (△) Q = 0.074 Å^{-1}; (●) Q = 0.093 Å^{-1}; (□) Q = 0.121 Å^{-1}. The solid lines are the result of a fit with the Ronca model.[7] The arrows indicate $Q^2l^2\sqrt{W\tau_e}$ for each curve.

to establish the Rouse regime. The obtained characteristic frequencies are also displayed in Figure 4. Properly limiting the time range agagain leads to excellent agreement with the Q^4 law. Furthermore we observe good agreement between the data sets taken at λ = 8.5 Å and λ = 11.8 Å, respectively. For the Rouse rate Wl^4 = (2.3 ± 0.1) × 10^{13} Å^4 s^{-1} is found. (In order to be short the term Rouse rate is also used for the product Wl^4 which is the model parameter of the Rouse model.)

We now analyze the full spectra with respect to deviations from Rouse relaxation at long times which are already evident in Figure 3. In order to scrutinize whether systematic deviations from the Rouse scaling behavior are present, Figure 5 displays the spectra obtained from sample 1 in a scaling representation using Wl^4 = 2.0 × 10^{13} Å s^{-1}, the value found from the short-time Rouse regime. For small values of the scaling variable u the data are reasonably well described by the Rouse master function (look, however, for the long-time results at Q = 0.064 Å^{-1}). Toward larger u the data fall systematically above the master function, indicating slower relaxation or the presence of constraints. Within experimental accuracy, however, the deviations from scaling are still marginal though slight indications for a splitting of the spectra with Q are suggestive. In this respect the spectra are similar to those obtained earlier from PDMS, where at larger values of the scaling variable a slowing down of the relaxation compared to Rouse behavior was seen. However, the Rouse scaling still appeared to be preserved.[15] The spectra obtained from sample 2 using a shorter neutron wavelength essentially agree with those from sample 1 and are therefore not displayed.

Figure 6 presents the spectra from sample 2 measured with λ = 11.8 Å, thereby increasing t_{max} by a factor of 2.7 to 46 ns. The spectra again are displayed in the scaling form. They deviate significantly from the Rouse scaling and exhibit a pronounced Q splitting. Due to the low intensity of the neutron beam at 11.8 Å, the data are somewhat noisy. However, the Q splitting amounts to several times the statistical error σ. The solid lines represent a fit with Ronca's effective medium model. The Rouse rate was fixed to the value obtained at short times using the λ = 8.5 Å spectra (Wl^4 = 2.3 × 10^{13} Å^4 s^{-1}). The only parameter fitted was the entanglement distance yielding d = 52 ± 1 Å. Overall, Ronca's model provides a good description of the experimental data concerning both the line shape as well as the magnitude of the Q splitting. Finally, using eqs 4a and 4b, we calculate the crossover time τ_e from unrestricted Rouse to entanglement-controlled behavior. The calculation on the basis $\Delta r_{nn}^2 = d^2$ (eq 4a) results in τ_e = 250 ns, clearly overestimating τ_e—in this case entanglement effects would have hardly been seen in the experimental time window (t_{max} = 46 ns). Equation 4b which calculates τ_e as the Rouse time of a chain between entanglements gives τ_e = 32 ns, which is compatible with the experimental spectra. Small arrows in Figure 6 indicate the position in the scaling plot where $Q^2l^2\sqrt{W\tau_e}$ is reached, showing that the experimental time range just reaches the crossover region.

4.2. Results on the Alternating Poly(ethylene-propylene) Copolymer. The experiments on PEP were carried out on two different polymers: (i) a homopolymer and (ii) a triblockcopolymer, where the inner third was protonated (see Table I). The NSE experiments were performed in a time window 0.5 ≤ t ≤ 37 ns (λ = 11.3 Å). Figure 7 displays the measured dynamic structure factors for the two polymers at T = 492 K. The scattering functions are characterized by a rapid initial decrease followed for longer times by a plateau regime in time. The observation of an "elastic" time-independent contribution to $S(Q,t)$ is the central result of this experiment. For comparison for the largest Q the dashed line in Figure 7 displays the dynamic structure factor for unrestricted Rouse relaxation exhibiting the same initial decay. A comparison of the homopolymer and triblock results shows that apart from a slightly slower relaxation in the initial decay the triblock has a similar relaxation behavior. In particular the long-time plateaus are identical for both polymers, indicating that they both relax under the same constraints—end effects appear to be of no importance.

Figure 8 presents the homopolymer data in a scaled form. The spectra were fitted jointly with Ronca's effective medium model and are plotted against the Rouse variable. The splitting into Q-dependent plateau levels is much more pronounced than for PI, a phenomenon resulting from a faster relaxation rate and somewhat stronger constraints. Again, the Ronca model represents an excellent description of the experimental data reproducing the line shape, i.e., the relatively sharp crossover and the Q dependence of the plateau levels. The results for the model parameters are given in Table II.

In order to test further for the internal consistency of the fitting routine, we fitted the entanglement distance d

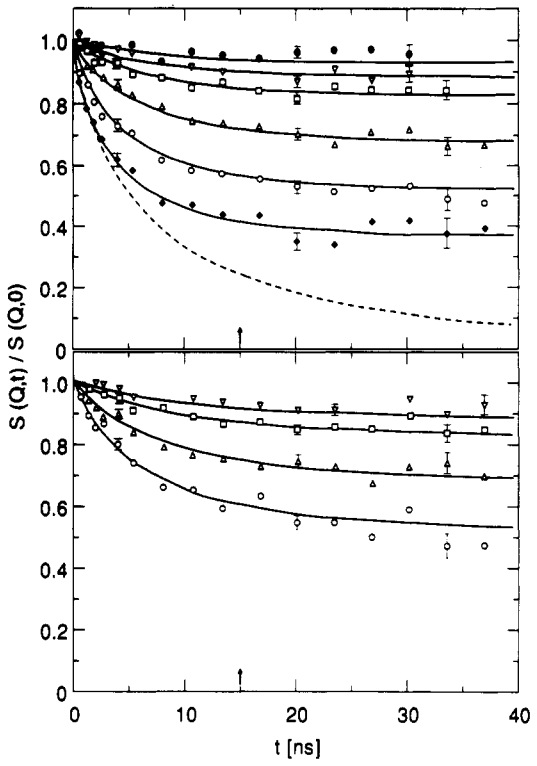

Figure 7. NSE spectra from the PEP homopolymer (upper part) and the triblock (lower part) at 492 K: (●) $Q = 0.058$ Å^{-1}; (▽) $Q = 0.068$ Å^{-1}; (□) $Q = 0.078$ Å^{-1}; (△) $Q = 0.097$ Å^{-1}; (○) $Q = 0.116$ Å^{-1}; (◆) $Q = 0.135$ Å^{-1}. The solid lines are the result of a fit with the Ronca model.[7] The dashed line presents the expected dynamic structure factor for Rouse relaxation corresponding to the highest Q value. The arrow marks the crossover time τ_e.

at different Q values separately. Table III presents the results. Within the experimental accuracy no significant Q dependence of the entanglement distance exists. Finally, the crossover time $\tau_e = 15$ ns (T 492 K) calculated with eq 4b agrees well with the observed spectral shape in dividing of the initial fast decay from the plateaulike behavior at longer times (see also arrows for $Q^2l^2\sqrt{W\tau_e}$).

In order to test De Gennes' local reptation model, we also have performed fits of the long-time tails of the spectra using eq 6—the local reptation model neglects the initial Rouse relaxation, therefore the initial part of the spectra has to be omitted. The time limit above which initial relaxation is not important is somewhat arbitrary. We required $t > \tau_e$ and cut the spectra at 17 ns considering only data points at larger times. Since the initial decay determining the Rouse relaxation rate is taken out, we imposed the rate obtained from the Ronca fit. Furthermore, in order to extend the fitting routine to higher Q values, the result of the first-order expansion in eq 6 $1 - (Qd/6)^2$ was replaced by $\exp(-(Qd/6)^2)$. Though the whole procedure is not unambiguous, we also obtained a good description of the long-time behavior (see Figure 8 lower part), indicating that the trends in the dynamic structure factor are depicted correctly. We note that with the given statistical accuracy of the data we are not in a position to distinguish between the models.

4.3. Saturated Polybutadiene, PEB-2. With respect to the intensity–resolution relationship of NSE, PEB-2 (essentially PE with one ethyl branch every 50 main chain bonds) has two advantages compared to PEP: (i) The Rouse rate Wl^4 of PEB-2 is more than 2 times faster than that of PEP at a given temperature (Wl^4_{PEP} (500 K) = 3.3×10^{13} Å^4 s^{-1}; Wl^4_{PEB} (509 K) = 7×10^{13} Å^4 s^{-1}). (ii) At the same time the topological constraints are stronger.

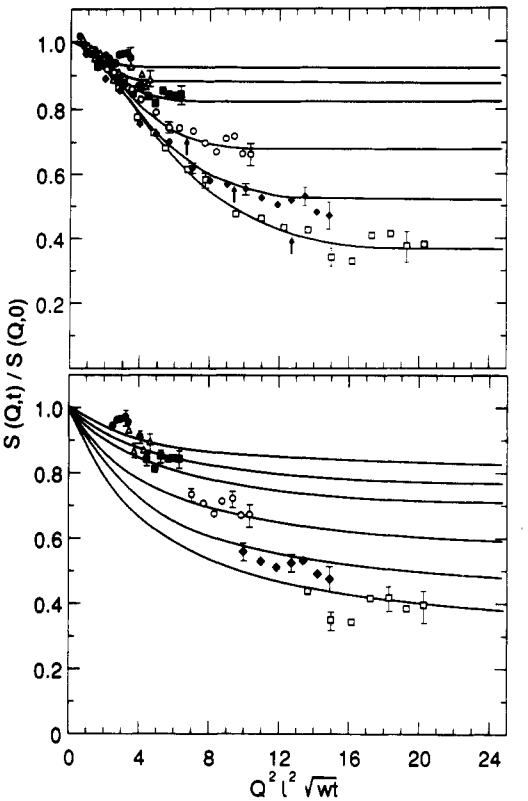

Figure 8. Rouse scaling representation of the PEP homopolymer data at 492 K: (upper part) solid lines represent the Ronca model;[7] (lower part) solid lines display the predictions of local reptation.[21] The solid lines from below to above correspond to $Q = 0.135$ Å^{-1}, $Q = 0.116$ Å^{-1}, $Q = 0.097$ Å^{-1}, $Q = 0.078$ Å^{-1}, $Q = 0.068$ Å^{-1}, $Q = 0.058$ Å^{-1}. The symbols along the lines are data points corresponding to the respective Q value. The arrows indicate $Q^2l^2\sqrt{W\tau_e}$ for the spectra at higher Q values.

Therefore it was possible to access the interesting time regime using neutrons of short wavelength ($\lambda = 8.5$ Å) covering the time window $0.3 \le t \le 17$ ns. The neutron intensity at this wavelength is about 4 times higher than that at $\lambda = 11.25$ Å used for PEP, leading to data of higher statistical accuracy.

The experiment was performed at $T = 509$ K. Figure 9 presents representative spectra in a scaling form. The solid line in the upper part of Figure 9 is the result of a fit with the Ronca model. As is evident, the agreement between the Ronca model and the experimental results is not as good as for the other two polymers; the spectra appear to exhibit some systematic deviations from the theoretical curves. For $Q = 0.078$ Å^{-1} and $Q = 0.116$ Å^{-1} at long times the data points fall below the theoretical line, while for $Q = 0.155$ Å^{-1} the opposite trend is evident.

Therefore, we investigated whether the De Gennes local reptation model (eq 6) is able to overcome the discrepancies. For this purpose, in order to determine the Rouse relaxation rate, we first evaluated the short-time part of the spectra. From fits of these data involving only one parameter, the Rouse rate or the related monomeric friction coefficient ζ was obtained. For the determination of ζ from $Wl^4 = 3kTl^2/\zeta$ we took $l^2 = C_\infty l_0^2 = 13.05$ Å^2 [29] (Table II).

When this Rouse rate was kept fixed, the long-time tails ($t \ge 7$ ns, $\tau_e = 5$ ns) of the spectra were then fitted with the dynamic structure factor of local reptation (eq 6). The lower part of Figure 9 displays the result. Apparently, the local reptation model fits the spectra significantly better than the Ronca model. In particular it accounts for the persisting gradual decay of $S(Q,t)/S(Q,0)$ even at

Table II
NSE Results on Polymer Melts

		NSE			rheology	
sample	T (K)	d (Å)	$10^9\zeta$ (dynes/cm)	τ_e (ns)	d (Å)	$10^9\zeta$ (dynes/cm)
PI 1	468		4.4 ± 0.3			1.2
PI 2	473	52 ± 1	3.8 ± 0.3	32	51 (298 K)	
PEP homopolymer	492	47.5 ± 0.4	3.1 ± 0.1	15	43.5 ± 2	1.9
PEP triblock	491	47.1 ± 0.7	2.4 ± 0.2	15		
PEB-2	509	43.5 ± 0.7[a]			35 (373 K) PE	0.3 (448 K)
		43.1 ± 0.9	0.4 ± 0.04	5	42 (509 K) PEB-7	

[a] Fit with local reptation.

Table III
Entanglement Distance from Fits of the Ronca Model to the Dynamic Structure Factor of PEP at Different Q Values[a]

Q (Å^{-1})	d (Å) homopolymer	d (Å) triblock
0.058	42 ± 2	
0.068	47.3 ± 1.9	47.3 ± 2.2
0.078	47.6 ± 0.9	46.2 ± 1.0
0.097	46.9 ± 0.5	47.0 ± 0.8
0.116	48.7 ± 0.5	47.8 ± 0.9
0.136	47.3 ± 0.6	

[a] The errors are only the statistical errors.

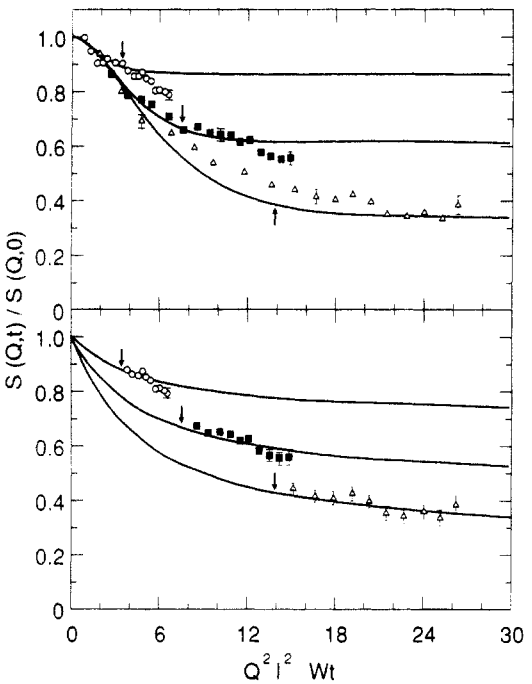

Figure 9. NSE spectra obtained from PEB-2 at 509 K in a Rouse scaling presentation: (○) $Q = 0.078$ Å^{-1}; (■) $Q = 0.116$ Å^{-1}; (△) $Q = 0.155$ Å^{-1}. The upper part displays the full spectra; the solid lines are a result from a fit with the Ronca model.[7] The lower part contains the data points for $t > \tau_e$. The solid lines represent the predictions of local reptation.[21] The arrows indicate $Q^2l^2\sqrt{W\tau_e}$ for each spectrum.

large $Q^2l^2\sqrt{Wt}$. Furthermore, it also describes the amount of Q splitting more accurately than the Ronca model. The resulting entanglement distance d from the fit with the local reptation model is also included in Table II. As can be seen, the values for d obtained from both models differ only slightly.

5. Discussion

The existence of a well-defined entanglement length in dense polymer systems so far has been inferred indirectly from macroscopic experiments like measurements of the plateau modulus. However, its direct microscopic observation remained impossible. The difficulty in directly evaluating the entanglement length is based on its very nature as a dynamic length scale which cannot be traced in static, structural investigations like small-angle scattering. Its observation needed dynamic experiments covering the relevant length and time scales. As discussed in section 2, an intermediate dynamic length scale should cause systematic Q-dependent deviations from Rouse scaling because besides the combination $l^2Q^2\sqrt{Wt}$ it introduces a second explicit Q dependence into the dynamic structure factor $S(Qd,Q^2l^2\sqrt{Wt})$. Figures 6 (PI), 8 (PEP), and 9 (PEB) display the "Q splitting" of $S(Q,t)$ for the three polymers investigated and prove directly the microscopic existence of an intermediate dynamic length scale which profoundly affects the relaxation of density fluctuations.

The observation of these systematic Q-dependent deviations from Rouse dynamics without applying specific models demonstrates the microscopic presence of the entanglement length scale. In order to arrive at quantitative results comparison with model predictions is necessary. Presenting the experimental results in the last section, we have shown fits of the obtained dynamic structure factors to the Ronca model[7]—and the local reptation model by De Gennes.[21] Though being an effective medium approach which treats the influence of the chain confinement heuristically in terms of a memory function, the Ronca model is appealing, because it is the only model providing an analytic form of $S(Q,t)$ in the crossover regime from Rouse dynamics to chain confinement. For times larger than τ_e, the crossover time from unrestricted Rouse motion to entanglement-controlled dynamics (eq 4) (but much smaller than the terminal time τ_d) it treats the chain essentially as elastically bound between entanglements. Therefore, at τ_e a sharp crossover to a plateau in $S(Q,t)$ is predicted. On the other hand the local reptation model of De Gennes describes the equilibration of density fluctuations along the fixed tube, thereby neglecting the initial unrestricted Rouse motion. Beyond the first strong decrease of $S(Q,t)$ due to unrestricted Rouse dynamics, the equilibration of density fluctuations by Rouse motion confined by the tube leads to a very gradual further decay of $S(Q,t)$ which may not easily be distinguished from the strict plateau in Ronca's approach. Only for times $\tau_R < t \ll \tau_d$ should a strict plateau occur.

For PI, where $\tau_e = 32$ ns lies at the outer edge of the experimental time window, a distinction between both models is impossible. Since most of the data points were taken for $t < \tau_e$, even a fit with the local reptation model, where the initial Rouse part ($t < \tau_e$) has to be excluded, is not feasable. The best that could be done was a description in terms of the Ronca model which depicts the crossover.

In the case of PEP the crossover time τ_e = 15 ns is situated in the center of the observation window (t_{max} = 36 ns). Both models, the Ronca and the local reptation model, were fitted and within statistical accuracy described the data equally well. For PEB-2 (τ_e = 5 ns) in terms of the τ_e we covered the largest time range ($t_{max} = 3.5\tau_e$) and also aquired the best statistical accuracy. There, the spectra clearly indicate deviations from a strict plateau behavior of $S(Q,t)$ beyond τ_e (Figure 9). Furthermore, also the Q dependence appears to be better accounted for by the local reptation model. These results show that the picture of an elastically bound chain—though describing the crossover properties quite well and resulting in very similar values for the entanglement distances—is an oversimplification which misses the slow density fluctuations along the tube predicted by the reptation model.

In the framework of reptation theory eq 7 relates the dynamical mechanical properties of a polymer melt expressed by the plateau modulus G_N^0 to the microscopic tube diameter describing the constraints of segmental motion. Table II compares tube diameters derived from plateau moduli[30] with the NSE results. For all three polymers the agreement between microscopic and macroscopic results is good. While for PI and PEP the agreement is nearly quantitative, the slightly larger difference for PEB-2 compared to PE may be related to the residual ethyl branches (2 for 100 main chain bonds) which cause some extra bulkiness. A comparison with the tube diameter derived from plateau moduli measurements on PEB-7 underlines this assertion. The coincidence of tube diameters determined macroscopically by application of the reptation model and direct microscopic results is far better than what could have been expected and strongly underlines the basic validity of the reptation approach.

As concerns the crossover time τ_e, we realized in equating τ_e with the aid of eqs 4a,b that a calculation on the basis of $\Delta r_{nn}^2 = d^2$ (4a) leads to an overestimation: In order for the entanglement constraints to become effective, a single chain segment needs to explore a region smaller than the tube diameter. Using the Rouse time of an entanglement strand as the appropriate estimate, we obtain good agreement with what can be estimated qualitatively from the crossover properties of the experimental line shape (Figures 6, 8, and 9). The ratio of the times determined by eqs 4a,b of $\pi^3/4$ yields $d^2/\Delta r_{nn}^2(\tau_e)$ = 2.8 or a single segment may travel a distance of about 60% of d before it is seriously affected by entanglements.

Recently, Kremer and Grest[22] published one of the most extensive molecular dynamics (MD) simulations on the dynamics of polymer melts. They studied ensembles of chains up to 150 beads which corresponded to about four entanglement lengths. Besides a study of the mean square segment displacements which very nicely display the crossover from a $t^{1/2}$ to a $t^{1/4}$ behavior, as predicted by reptation, they also investigated the dynamic structure factor.

In order to compare the MD simulations with experiments, a mapping procedure had to be developed. Thereby, it was realized that a transcription of the persistence length did not suffice and it was argued that appropriate mapping may be achieved if the entanglement distance of the real polymer is identified with that of the computer polymer. For the computer polymer d or N_e, the number of monomers in an entanglement strand was essentially determined from the $t^{1/2}$–$t^{1/4}$ crossover in conjunction with the assumption that τ_e is the Rouse relaxation time of a polymer with N_e monomers. This assumption led to consistent results for the various dynamical quantities and

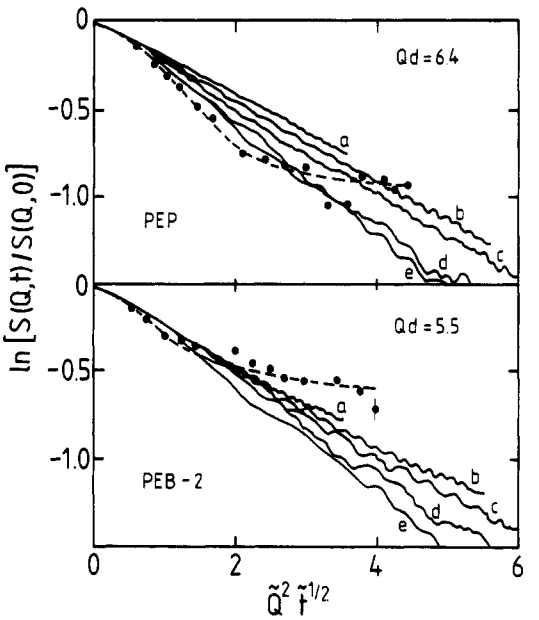

Figure 10. Comparison of the experimental dynamic structure factors for PEP at Q = 0.135 (Qd = 6.4) and PEB-2 at Q = 0.128 Å^{-1} (Qd = 5.5) with the dynamic structure factors from the computer polymer. The various full lines respresent MD results for different Qd = 3.1 (a), 3.9 (b), 4.6 (c), 6.2 (d), and 7.7 (e). In the upper part the computer results are the structure factors from a fully labeled chain, while in the lower part only the center 35 monomers are labeled.

is also in agreement with our findings for τ_e explained above. The time scale in the mapping procedure is set by the crossover time τ_e or equivalently by a basic time τ which stays in a fixed proportion to τ_e.[31] If one measures Q in units of d and the time in units of τ_e, then a scattering function of the form $S(Qd,Q^2l^2\sqrt{Wt})$ transforms into $S(\tilde{Q},\tilde{Q}^2\sqrt{\tilde{t}})$ which should be universal. In this transformation the step length of the random-walk drops out. With this approach they successfully mapped properties of the computer polymer to real systems.

Using the mapping procedure in Figure 10, we compare the experimental dynamic structure factors for PEP and PEB-2 with the MD results on N = 150 chains. Figure 10a displays the MD result for different Qd—$S(Q,t)$ was calculated by averaging over all monomers of the chain—with the appropriately scaled experimental spectrum taken on PEP at Q = 0.135 Å^{-1} and T = 492 K (Qd = 6.4). Figure 10b presents a similar comparison now with a PEB-2 spectrum (Q = 0.128 Å^{-1}, T = 509 K, Qd = 5.5) with the same MD result, where $S(Q,t)$ was obtained by averaging over the innermost 35 beads.[22] Obviously, experimental spectra and MD results disagree strongly. While the experimental results show a strong tendency to bend away from the initial Rouse relaxation, thereby crossing over to near plateau values, and to split with Q (Figures 8 and 9), the MD-generated spectra display only marginal traces of such a behavior. At larger values of the scaling variable the MD spectra in Figure 10b resulting from the inner segments exhibit some slight tendencies to split and to plateau. It is interesting to note that the mean square displacement of the inner segments in these computer polymers undergoes a sharp well-defined $t^{1/2}$–$t^{1/4}$ crossover, while the dynamic structure factor even for the inner segments is far from what is observed for long chains. Presently, we think that the discrepancy results from too short chains in the MD simulation. Seemingly, the pair correlation function, even if it is only taken for the center part of the chains, is more sensitive to finite size effects

like constraint release or tube length fluctuations than the self-correlation function.

6. Conclusion

The objective of this work was to study the effect of topological interaction on the dynamics of long-chain polymers in the melt on a molecular level. Using neutron spin echo, we accessed the polymer motion simultanously in space and time. We presented experiments on melts of PI, PEP, and PEB. The pertinent results may be summarized as follows. The measured dynamic structure factors on all three polymers show that beyond a characteristic time the relaxation of the pair correlation is strongly impeded. From the dependence on the momentum transfer an associated dynamic length can be extracted. We emphasize that the existence of this dynamic length reveals itself from systematic Q-dependent deviations from Rouse scaling. For the studied polymers this dynamic length is found to be on the order of 50 Å; much larger than a segment length but smaller than the chain dimensions. This finding establishes the existence of a microscopic intermediate dynamic length in polymer melts. A comparison with viscoelastic data on the plateau modulus which were evaluated in terms of reptation reveals good agreement between the directly measured microscopic length and the entanglement distance inferred from rheology. The microscopic motion can be best described in terms of the local reptation model of De Gennes while the model of an elastically trapped chain is less successful. A comparison with MD simulations reveals strong discrepancies which can be most likely traced to the short chains used in the simulations.

References and Notes

(1) Ferry, J. D. *Viscoelastic Properties of Polymers*; Wiley: New York, 1980.
(2) Doi, M.; Edwards, S. F. *The Theory of Polymer Dynamics*; Clarendon: Oxford, U. K., 1986.
(3) De Gennes, P. G. *Scaling Concepts in Polymer Physics*; Cornell University Press: Ithaca, NY, 1979.
(4) De Gennes, P. G. *J. Chem. Phys.* **1971**, *55*, 572.
(5) Doi, M.; Edwards, S. F. *J. Chem. Soc., Faraday Trans. 2* **1978**, *74*, 1789; **1978**, *74*, 1802; **1978**, *75*, 38.
(6) Scher, H.; Schesinger, M. F. *J. Chem. Phys.* **1986**, *84*, 5922.
(7) Ronca, G. *J. Chem. Phys.* **1983**, *79*, 1031.
(8) Skolnick, J.; Yares, R.; Kolinski, A. *J. Chem. Phys.* **1988**, *88*, 1407; **1988**, *88*, 1418.
(9) Hess, W. *Macromolecules* **1986**, *19*, 1395; **1987**, *20*, 2589; **1988**, *21*, 2620.
(10) Fixman, M. *J. Chem. Phys.* **1988**, *89*, 3892; **1988**, *89*, 3912.
(11) Schweizer, K. G. *J. Chem. Phys.* **1989**, *91*, 5802, 5822.
(12) Des Cloiseaux, J. *Macromolecules* **1990**, *23*, 4678.
(13) Higgins, J.; Roots, J. F. *J. Chem. Soc., Faraday Trans. 2* **1985**, *81*, 757.
(14) Richter, D.; Baumgärtner, A.; Binder, K.; Ewen, B.; Hayter, J. B. *Phys. Rev. Lett.* **1981**, *47*, 109; **1982**, *48*, 1695.
(15) Richter, D.; Ewen, B.; Farago, B.; Wagner, T. *Phys. Rev. Lett.* **1989**, *62*, 2140.
(16) Richter, D.; Farago, B.; Fetters, L. J.; Huang, J. S.; Ewen, B.; Lartigue, C. *Phys. Rev. Lett.* **1990**, *64*, 1389.
(17) Butera, R.; Fetters, L. J.; Huang, J. S.; Richter, D.; Pyckhout-Hintzen, W.; Zirkel, A.; Farago, B.; Ewen, B. *Phys. Rev. Lett.* **1991**, *66*, 2088.
(18) See e.g.: Mezei, F. In *Lecture Notes in Physics*; Mezei, F., Ed.; Springer Verlag: Berlin, Heidelberg, New York, 1980; Vol. 128.
(19) Rouse, P. E. *J. Chem. Phys.* **1953**, *21*, 1273.
(20) De Gennes, P. G. *Physics (Long Island City, N.Y.)* **1967**, *3*, 37.
(21) De Gennes, P. G. *J. Phys. (Paris)* **1981**, *42*, 735.
(22) Kremer, K.; Grest, G. S. *J. Chem. Phys.* **1990**, *92*, 5057.
(23) Kremer, K.; Grest, G. S.; Carmesin, I. *Phys. Rev. Lett.* **1988**, *61*, 566.
(24) Graessley, W. W. *Adv. Polym. Sci.* **1974**, *16*, 1.
(25) Hattam, P.; Gauntlett, S.; Mays, J. W.; Hadjichristidis, N.; Young, R. N.; Fetters, L. J. *Macromolecules* **1991**, *24*, 6199.
(26) Gotro, J. T.; Graessley, W. W. *Macromolecules* **1984**, *17*, 2767.
(27) Pearson, D. S.; Ver Strate, G.; von Merwall, E.; Schilling, F. C. *Macromolecules* **1987**, *20*, 1133.
(28) Rachapudy, H.; Smith, G. G.; Raju, V. R.; Graessley, W. W. *J. Polym. Sci., Polym. Phys. Ed.* **1979**, *17*, 1211.
(29) Boothroyd, A. T.; Rennie, A. R.; Boothroyd, C. B. *Europhys. Lett.* **1991**, *15*, 715.
(30) The plateau moduli for PI and PE were taken from ref 25; the modulus for PEP originates from ref 17; the value for PEB-7 was taken from: Carella, J. M.; Graessley, W. W.; Fetters, L. J. *Macromolecules* **1984**, *17*, 2775.
(31) According to the prescription in ref 22 the basic time was obtained from $\tau = \zeta_\mu \sigma^2/25kT = d^4/17500Wl^4$.

Registry No. PI, 9003-31-0; neutron, 12586-31-1.